Article

Analysis of Wind Field Response Characteristics of Tethered Balloon Systems

Ce Pang [1,2], Zeqing He [1,*], Kaiyin Song [1,2] and Shenghong Cao [1,2]

1   Aerospace Information Research Institute, Chinese Academy of Sciences, Beijing 100094, China; songkaiyin21@mails.ucas.ac.cn (K.S.)
2   University of Chinese Academy of Sciences, Beijing 100190, China
*   Correspondence: zqhe@aoe.ac.cn

Abstract: Tethered balloon systems encounter various complex wind field environments during flight. To investigate the conditions under which the system can operate safely and smoothly, a longitudinal dynamic model for tethered balloon systems is established. The model incorporates a streamlined balloon shape with its aerodynamic center at the body's center. Steady-state aerodynamic force coefficients are calculated through simulations and fitted to a function based on the angle of attack within a specified range. The complex cable model is simplified using the lumped mass method, considering the influence of branch cables on the main node position. Experimental results from windless oscillation tests on scaled tethered balloon systems are compared with numerical solutions obtained using the dynamic model under the same conditions, validating the feasibility of the model for simulating different wind field scenarios. Finally, the motion characteristics of tethered balloon systems in different wind fields are analyzed. The numerical simulation results show that in a horizontal step wind field, the cable tension and cable inclination angle increase with the wind speed, and the slower the wind field changes, the shorter the time required for system stabilization. Updrafts greatly increase the likelihood of balloon escape, while downdrafts greatly increase the likelihood of the system making contact with the ground. The findings of this study can provide a basis for selecting suitable wind field conditions and issuing risk warnings for tethered balloon systems.

Keywords: tethered balloon; wind field response; aerial vehicle; updraft; downdraft

1. Introduction

In recent years, tethered balloons have been shown to exhibit exceptional stability over the course of their time in the air, and are widely utilized in meteorological surveys, ground monitoring, and wireless communication [1–5]. Tethered balloons are typically connected to a ground anchor through a photoelectric composite cable [6,7], with the anchor remaining in a fixed position.

Because the tethered balloon is only constrained by the main cable, and the cable is also subject to gravity and aerodynamic forces, the tension of the cable gradually increases from the ground winch to the point where it connects with the balloon (the main node), and the cross-section of the cable at the main node is the most hazardous point of the cable [8]. The length and diameter of the cable are limited by weight and other factors, which ultimately causes the tension at the hazardous section of the cable to exceed a certain value, causing the cable to break and the balloon to escape [9]. The risk of system touchdown increases when the main node of a tethered balloon system is displaced too far in the wind field. To reduce the cable tension and the displacement of the main node in the wind field, several scholars have studied the dynamics of the tethered balloon system. H.M. Costello [10] and others investigated the law of influence of a tether with an aerodynamic cross-section on the response of a tethered balloon system in a wind field and proved its feasibility to reduce the tension of the tether cable concerning the displacement of

the main tether point. Jiang [11] analyzed the influence law of different tail configurations on the aerodynamic characteristics of the tethered balloon from the sphere structure, and it was found that the smaller the aerodynamic resistance of the sphere, the smaller the cable tension and the main tethering point displacement under the same wind field environment. Li [9] performed a simulation analysis of the response of a tethered balloon system to sudden gust disturbances and conducted a wind resistance performance analysis of the system. Surjit S. Badesha [12] analyzed the dynamical response of a tethered balloon system in a thunderstorm environment. Dipayan Mukherjee [13] analyzed the factors affecting the cable tension and swing amplitude during the ascent and descent of a tethered balloon system. Zhang [14] studied the effects of the aerodynamic coefficients of balloons and cables on the cable tension in stratospheric tethered balloon systems. G. S. Aglietti [15] studied the dynamic response of a high-altitude tethered balloon system in gusty winds and concluded that the response amplitude of a tethered balloon system in a steady-state wind field is larger than that of a tethered balloon system in a gusty wind field.

Currently, the wind field analysis of tethered balloon systems with a streamlined sphere is not fully understood, especially the effect of different wind directions on the response of the system. This paper investigates the effect of different wind directions on a tethered balloon system. The tethered balloon selected for this study has an "upside-down Y" tail fin, which exhibits a significant weathervane effect. The balloon primarily moves within the wind direction's plane, so this study focuses on analyzing the motion of the tethered balloon system in a two-dimensional plane. A dynamic model of the tethered balloon system in the longitudinal plane was established and simulated, and the dynamic response of the system was investigated in different maximum amplitude step changes, rates of change in wind speed, and vertical airflow. By analyzing the time domain response of key system parameters such as the tension and position at the main node, as well as the pitch angle of the balloon, suitable wind field environments for the tethered balloon system's stationary operation are identified, providing a basis for risk assessment. The remaining sections of this article are organized as follows: Section 2 presents the physical model of the tethered balloon system during stationary operation, providing a detailed analysis and calculation of the external forces acting on the balloon and constructing a simplified mathematical model of the system. Section 3 compares a series of experimental results of scaled tethered balloon systems with numerical simulation results to validate the accuracy of the mathematical model presented in Section 2. Subsequently, numerical simulations are conducted to analyze the dynamic response of a specific tethered balloon system in different wind field environments. Finally, Section 4 summarizes this research.

2. Dynamic Model

To study the motion of a tethered balloon system in different longitudinal wind fields, it is necessary to establish the longitudinal dynamics model of the system. Due to the flexible nature of the tether, its motion in the wind field is quite complex. Pastor-Rodríguez A [16] modeled the dynamics of a high-altitude kite system similar to that of a tethered balloon system in which the cable is treated as a multi-segmented massless rigid bar, which deviates significantly from the real system. Zhang [17] applied a multi-rigid connection structure to model the dynamics of an unmanned aircraft system with a parachute. In this study, a lumped mass model is adopted as a simplified model for accuracy and computational efficiency, and is widely used in dynamic calculations of complexly loaded ropes [18]. The tether model consists of multiple interconnected, straight, elastic, and massless cylindrical segments, with the mass concentrated at the connections and the aerodynamic forces acting at the midpoint of each segment. The deformation of the tether during the stationary motion of the balloon is neglected, and it is treated as a rigid body, with buoyancy and gravity acting at a fixed point. Figure 1 depicts the simplified model of the tethered balloon system. The inertial coordinate system is established with the tether winch as the origin. The *x*-axis is perpendicular to the line connecting the winch point and the center of the Earth, and it is parallel to the wind field plane. The *y*-axis is parallel

to the wind plane and points towards the sky. The body coordinate system is established at the center of the balloon, where the angle between the axes of the body coordinate system and the ground inertial coordinate system is referred to as the pitch angle and denoted by θ. The inertial coordinate system can be aligned with the body coordinate system by rotating counterclockwise within the longitudinal plane of the balloon. The transformation matrix is as follows:

$$\boldsymbol{L'} = \begin{bmatrix} \cos\theta & \sin\theta \\ -\sin\theta & \cos\theta \end{bmatrix} \tag{1}$$

The spatially distributed tethers are simplified as a two-dimensional planar configuration, as shown in Figure 2. In this simplification, we do not consider the mass and stretching deformation of the branch cables. Assuming that the tethers are straightened, the angles between the branch cable near the ball head and ball tail concerning the $o_b x_b$ axis are denoted as β_1 and β_2. The angle between the main tether and $o_b x_b$ axis is denoted as β. When $\beta_1 < \beta < \beta_2$, point P represents the rotation connection point between the balloon and the main tether. When $\beta < \beta_1$, point P_1 serves as the rotation point. Similarly, when $\beta_2 < \beta$, point P_2 acts as the rotation point.
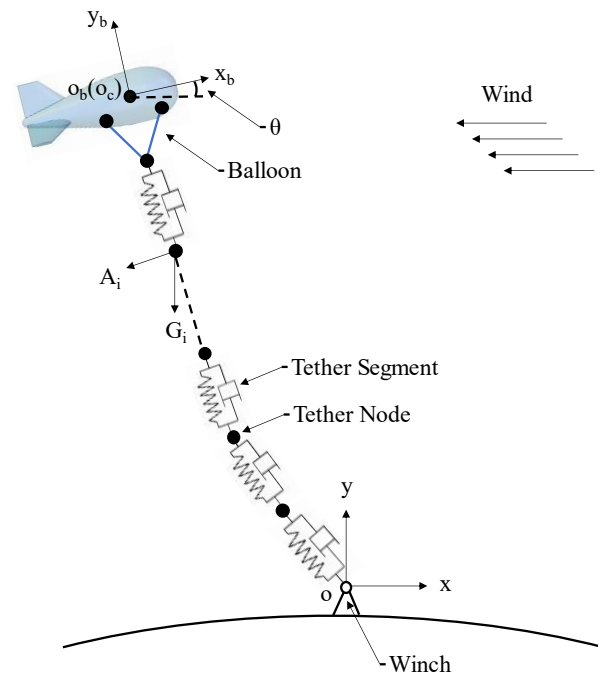

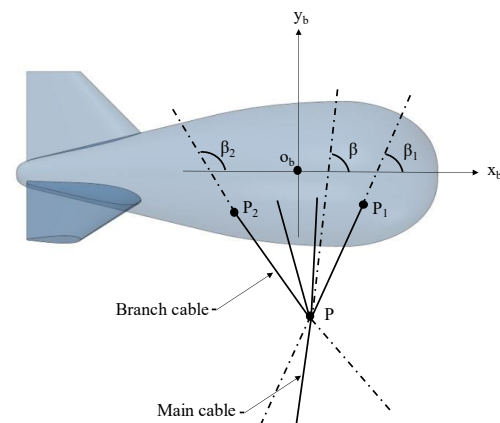**Figure 1.** Simplified model of tethered balloon system.

Figure 2. Rotation point change indication.

2.1. Balloon Dynamics Analysis

In the balloon body coordinate system, the expressions for the momentum "a" and the angular momentum "b" of the balloon are as follows:

$$p = m(V_K + \omega \times R_G) \tag{2}$$

$$L = I\omega + mR_G \times V_K \tag{3}$$

where $V_K = \begin{bmatrix} u & v \end{bmatrix}^\top$ denotes the velocity of the center of the balloon relative to the inertial coordinate system, ω is the angular velocity of the balloon's rotation, $R_G = \begin{bmatrix} R_{Gx} & R_{Gy} \end{bmatrix}^\top$ represents the position vector of the center of mass in the body coordinate system, and I is the moment of inertia tensor of the balloon about the body center in the body coordinate system.

According to the principles of rigid body momentum and angular momentum, the following equations can be derived:

$$\left(\frac{dp}{dt}\right)_b + \omega \times p = G + B + T + F_a \tag{4}$$

$$\left(\frac{dL}{dt}\right)_b + \omega \times L + V_K \times p = M_G + M_B + M_T + M_a \tag{5}$$

where $\left(\frac{d}{dt}\right)_b$ denotes the time derivative of the variables observed in the body coordinate system, G and M_G represent the gravity and gravitational moment acting on the balloon, B and M_B represent the buoyancy and buoyancy moment acting on the balloon, T and M_T represent the tension and tension moment of the tether acting on the balloon, F_a and M_a represent the aerodynamic force and aerodynamic moment acting on the balloon. The external force on the balloon is shown in Figure 3.

The force and moment equations for gravity in the body coordinate system during the stationary flight of the balloon are as follows:

$$G = L' \begin{bmatrix} 0 \\ -m_{ball}g \end{bmatrix} = \begin{bmatrix} G_x \\ G_y \end{bmatrix} \tag{6}$$

$$M_G = G_x \times R_{Gy} - G_y \times R_{Gx} \tag{7}$$

where g is the acceleration due to gravity and m_{ball} represents the combined mass of the tethered balloon's skin and payload.

In the body coordinate system, the equations for calculating the buoyant force and buoyant moment acting on the balloon are as follows:

$$B = L' \begin{bmatrix} 0 \\ (\rho_A - \rho_b)g V_b \end{bmatrix} = \begin{bmatrix} B_x \\ B_y \end{bmatrix} \tag{8}$$

$$M_B = B_x \times R_{By} - B_y \times R_{Bx} \tag{9}$$

where ρ_A represents the atmospheric density at the altitude where the tethered balloon is located, ρ_b represents the average density of helium in the main envelope of the tethered balloon and the air in the auxiliary envelope, V_b represents the volume of the tethered balloon during stationary operation, and $R_B = \begin{bmatrix} R_{Bx} & R_{By} \end{bmatrix}^\top$ represents the position vector of the buoyant center in the body coordinate system.

In the body coordinate system of the balloon, the equations for calculating the tension and tension moment of the main tether are as follows:

$$T = \begin{bmatrix} T_x & T_y \end{bmatrix}^\top \tag{10}$$

$$M_B = T_x \times R_{Ty} - T_y \times R_{Tx} \tag{11}$$

where $\boldsymbol{R_T} = \begin{bmatrix} R_{Tx} & R_{Ty} \end{bmatrix}^\top$ is the position vector of the connection point between the balloon and the main mooring cable in the volume coordinate system.

Due to the relative velocity of the tethered balloon concerning the airflow generally being below 20 m/s, the flow field around the tethered balloon system during stationary flight can be approximated as an incompressible flow field. In the stationary flight process of the tethered balloon, the majority of the time is characterized by unsteady motion. During the unsteady motion of the tethered balloon, the aerodynamic forces and moments depend not only on the angle of attack, flight velocity, and air density but also on the derivatives of these parameters concerning time. To accurately calculate the aerodynamic forces experienced by the balloon during motion, the aerodynamic force coefficients are divided into three parts: steady-state aerodynamic forces, dynamic derivatives, and added masses.

Steady-state aerodynamic forces and dynamic derivatives can be calculated using a unified formula. The calculation formula is

$$\boldsymbol{F_a} = \begin{bmatrix} F_l \\ F_d \end{bmatrix} = \begin{bmatrix} (C_l + C_l'\omega_z)qS \\ (C_d + C_d'\omega_z)qS \end{bmatrix} \tag{12}$$

$$M_A = (C_m + C_m'\omega_z)qV_b \tag{13}$$

where F_l, F_d, and F_m represent the aerodynamic lift, drag, and pitching moment experienced by the balloon, excluding the added mass. C_l, C_d, and C_m represent the steady-state lift coefficient, drag coefficient, and pitching moment coefficient. C_l', C_d', and C_m' represent the lift coefficient term, drag coefficient term, and pitching moment coefficient term of the dynamic derivatives. $q = \frac{1}{2}\rho_A|V_\Lambda|^2$ represents the dynamic pressure acting on the balloon. S represents the characteristic area of the tethered balloon. V_b represents the volume of the tethered balloon. ω_z is the rotation speed of the balloon relative to the wind field. As shown in Figure 3.
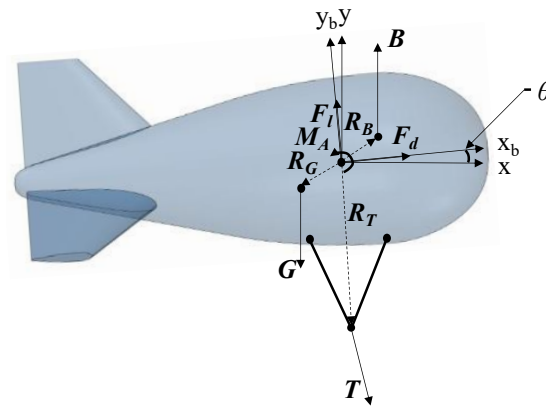

Figure 3. Balloon force.

For the calculation of the steady-state aerodynamic coefficients, the steady-state aerodynamic forces were first calculated by CFD for a range of angles of attack. Let C_l' and C_d' be zero and invert the steady-state aerodynamic coefficients via Equations (12) and (13). A continuous function of the aerodynamic coefficients concerning the angle of attack is fitted by a polynomial.

To accurately calculate the steady-state aerodynamic forces acting on the tethered balloon in the longitudinal plane, a simulation range of $-\pi$ to π is chosen for the angle of attack. The steady-state aerodynamic coefficients were then fitted using the least squares method to obtain a polynomial function with the angle of attack as an independent variable that minimizes the sum of the squares of the errors between the simulated and fitted values. Equation (14) represents the fitting equation for the aerodynamic force coefficients. Table 1 shows the polynomial coefficients of the fitted equations for the aerodynamic coefficients. Table 2 shows that the mean absolute error (MAE) of the aerodynamic simulation and the

fitting of the balloon do not exceed 0.13 and the root mean square error (RMSE) does not exceed 0.24. Figure 4 depicts that the fitted function closely matches the aerodynamic force coefficients obtained from the CFD calculations.

$$C_i = a_0 + a_1 x + a_2 x^2 + a_3 x^3 + \dots \quad i = l, d, m \tag{14}$$

Table 1. Polynomial coefficients for the balloon aerodynamic coefficient fitting equation.

	C_l	C_d	C_m
a_0	-0.01738	-0.02959	7.619×10^{-3}
a_1	0.02925	3.02×10^{-4}	-4.99×10^{-3}
a_2	4.082×10^{-5}	1.169×10^{-4}	-2.246×10^{-5}
a_3	-2.148×10^{-6}	1.041×10^{-7}	-3.623×10^{-7}
a_4	-2.507×10^{-9}	-7.532×10^{-9}	8.454×10^{-10}
a_5	5.951×10^{-11}	-4.566×10^{-12}	1.641×10^{-11}
a_6	3.765×10^{-14}	1.236×10^{-13}	
a_7	-6.211×10^{-16}		

Table 2. Simulation of balloon aerodynamic coefficients with fitting errors.

	MAE	RMSE
C_l	0.0417	0.0533
C_d	0.0532	0.1119
C_m	0.0527	0.0799
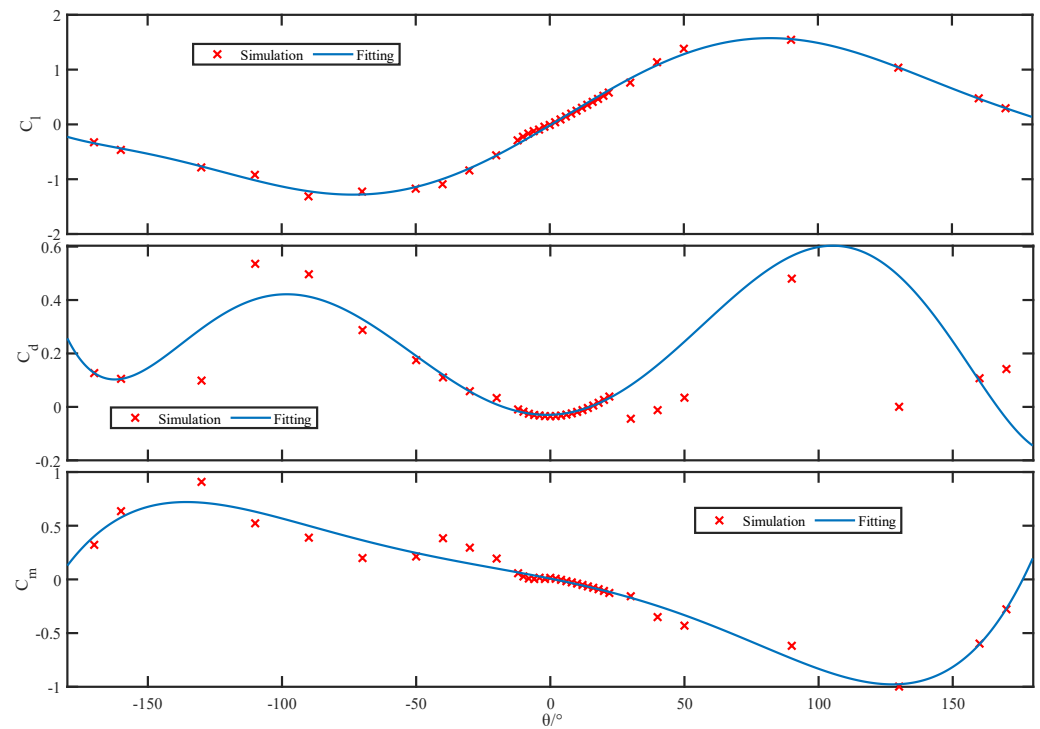
Figure 4. Steady-state aerodynamic coefficient.

The aerodynamic force dynamic derivatives can be simplified as a function of the tethered balloon's relative wind rotation speed. The calculation formula is as follows:

$$\begin{cases} C'_d = 0 \\ C'_l = 1.8 C_y^\alpha \frac{S_e L_{r,o}}{SL} \\ C'_m = -1.8 C_y^\alpha \frac{S_e L_{r,o}{}^2}{SL^2} \end{cases} \tag{15}$$

where C_y^α is the rotation speed of the balloon relative to the wind field, S_e represents the horizontal reference area of the tail fin, $L_{r.o}$ represents the horizontal distance from the aerodynamic center of the horizontal tail to the body center, and L represents the characteristic length of the balloon.

This article focuses on the motion of the tethered balloon system in the longitudinal plane. The estimation involves calculating the added mass in the $o_b x_b$-axis and $o_b y_b$-axis directions, as well as the added rotational inertia around the $o_b z_b$-axis. The calculation of the added mass for the balloon can be divided into two parts: the added mass of the balloon body and the added mass of the tail fin. The additional mass coefficient in the longitudinal plane of the tethered balloon body is calculated according to the following formula [19]:

$$\begin{cases} l_{eq} = \frac{\pi L^2}{4S_m} \\ e = \sqrt{1 - l_{eq}^{-2}} \\ \alpha_0 = \frac{1-e^2}{e^3}\left[\ln\left(\frac{1+e}{1-e}\right) - 2e\right] \\ \beta_0 = \frac{1}{e^2} - \frac{1-e^2}{2e^3}\ln\left(\frac{1+e}{1-e}\right) \end{cases} \tag{16}$$

$$\begin{cases} k_x = \frac{\alpha_0}{2-\alpha_0} \\ k_y = \frac{\beta_0}{2-\beta_0} \\ k_3 = \left(\frac{b^2-a^2}{b^2+a^2}\right)^2 \frac{\alpha_0 - \beta_0}{2\left(\frac{b^2-a^2}{b^2+a^2}\right)+(\beta_0-\alpha_0)} \end{cases} \tag{17}$$

$$\begin{cases} m_{1x} = m_{air}k_x \\ m_{1y} = m_{air}k_y \\ I_{1z} = \frac{a^2+b^2}{5}I_{air}k_3 \end{cases} \tag{18}$$

where m_{air} and I_{air} represent the mass and moment of inertia of the air displaced by the balloon body, respectively; S_m represents the cross-sectional area of the tethered balloon's body in the meridional plane; a and b represent the major and minor axes of the equivalent ellipse for the balloon's body, respectively.

Due to the relatively small projected area of the tail fin in the $o_b x_b$-axis direction, it can be approximated as a thin plate with no thickness. The calculation formula for the added mass of the tail fin is

$$\begin{cases} m_{2x} = 0 \\ m_{2y} = \pi\rho\int_c r_1^2(1 - \frac{2r_2^2}{r_1^2} + \frac{r_2^4}{r_1^4})dx \\ I_{2z} = \pi\rho\int_c x^2 r_1^2(1 - \frac{2r_2^2}{r_1^2} + \frac{r_2^4}{r_1^4})dx \end{cases} \tag{19}$$

where r_1 represents the distance between the end of the balloon's tail fin and the centerline of the main envelope, r_2 represents the average distance between the connection point of the tail fin with the main envelope and the centerline of the main envelope, and c represents the average aerodynamic chord length of the tail fin.

Based on the above, the added mass of the balloon can be expressed as

$$\begin{cases} m_x^{add} = m_{1x} + m_{2x} \\ m_y^{add} = m_{1y} + m_{2y} \\ I_z^{add} = I_{1z} + I_{2z} \end{cases} \tag{20}$$

2.2. Cable Dynamics Analysis

In the analysis of the tethered balloon system, the main tether cable is treated using the lumped mass method. The cable is discretized into n segments, and the mass of each segment is concentrated at a single point. The gravitational force acting on each mass point can be calculated as

$$G_i = \rho_c L_i \tag{21}$$

where ρ_c represents the linear density of the tether cable, and L_i represents the length of the ith segment of the tether cable.

The formula for calculating the tension along the line connecting adjacent mass points is as follows:

$$|T_i| = \begin{cases} AE\varepsilon_i + \eta\dot{\varepsilon}_i & \varepsilon_i > 0 \\ 0, & \varepsilon_i \leq 0, \ AE\varepsilon_i + \eta\dot{\varepsilon}_i < 0 \end{cases} \tag{22}$$

where A represents the initial cross-sectional area of the tether cable, E represents the elastic modulus of the material used for the tether cable, η represents the cable damping, and $\varepsilon_i = (L_i - L_{iu})/L_{iu}$ represents the strain of the tether cable segment.

To calculate the aerodynamic forces on the tether cable in the wind field, each segment of the cable is considered a cylinder. As shown in Figure 5, the schematic diagram represents the aerodynamic forces acting on the ith segment of the cable. The airspeed at the midpoint of the cable can be calculated as

$$V_i = V_i^c - V_i^{wd} \tag{23}$$

where V_i^c represents the absolute velocity at the midpoint of each cable segment, and V_i^{wd} represents the wind velocity at each cable segment.
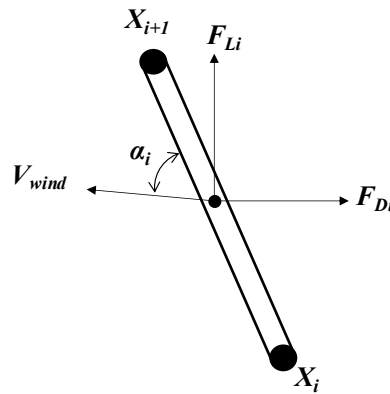

Figure 5. Aerodynamic forces on the micrometric segments of the cable.

The calculation formulas for the lift coefficient and drag coefficient of an inclined cylinder [20] are as follows:

$$\begin{cases} C_D^i = C_{Df} + C_{Dbasic}\sin^3\alpha_i \approx 0.022 + 1.1\sin^3\alpha_i \\ C_L^i = C_{Dbasic}\sin^2\alpha_i\cos\alpha_i \approx 1.1\sin^2\alpha_i\cos\alpha_i \end{cases} \tag{24}$$

The cable angle of attack is calculated as follows:

$$\alpha_i = \arccos\left(\frac{(X_{i+1} - X_i)\cdot V_i}{|X_{i+1} - X_i||V_i|}\right) \tag{25}$$

The direction of lift e_L^i and the direction of drag e_D^i of the ith section of the cable are determined by the following equation:

$$\begin{cases} e_D^i = -\frac{V_i}{|V_i|} \\ e_L^i = \frac{k\times V_i}{|V_i|} \end{cases} \tag{26}$$

where k is a unit vector perpendicular to the longitudinal plane.

The aerodynamic lift and aerodynamic resistance of the ith section of the cable are calculated as

$$\begin{cases} F_D^i = \frac{1}{2}\rho C_D^i l_i d|V_i|^2 e_D = -\frac{1}{2}\rho C_D^i l_i d|V_i|(v_{xi}\boldsymbol{i} + v_{yi}\boldsymbol{j}) \\ F_L^i = \frac{1}{2}\rho C_L^i l_i d|V_i|^2 e_L = \frac{1}{2}\rho C_L^i l_i d|V_i|(-v_{yi}\boldsymbol{i} + v_{xi}\boldsymbol{j}) \end{cases} \tag{27}$$

The equilibrium equations for the dynamics of the *i*th mass in the inertial system are as follows:

$$\boldsymbol{T_{i+1}} - \boldsymbol{T_i} + \boldsymbol{G_i} + (\boldsymbol{F_D^i} + \boldsymbol{F_D^{i+1}})/2 + (\boldsymbol{F_L^i} + \boldsymbol{F_L^{i+1}})/2 = m\frac{d^2\boldsymbol{r_i}}{dt^2} \tag{28}$$

2.3. Dynamical Modeling of Tethered Balloon Systems

The tethered balloon dynamics equations are obtained by coupling the cable dynamics equations and the balloon dynamics equations. The position vector of the main node of the balloon in the ground coordinate system is the same as the position vector of the n$^{\text{th}}$ mass point of the cable in the ground coordinate system, and the tension force on the balloon at the main node is equal in magnitude and opposite in direction to the tension force on the cable at the main node, as follows:

$$\boldsymbol{T} = -\boldsymbol{L'}\boldsymbol{T_{i+1}} \tag{29}$$

The following equation shows the differential equation for the longitudinal dynamics of the tethered balloon system:

$$\begin{cases} \frac{du}{dt} + R_{Gy}\frac{d\omega}{dt} + \omega v = (G_x + B_x + T_x + F_d)/(m_{he} + m_{ball} + m_x^{add}) \\ \frac{dv}{dt} - R_{Gx}\frac{d\omega}{dt} - \omega u - R_{Gy}\omega^2 = (G_y + B_x + T_y + F_l)/(m_{he} + m_{ball} + m_y^{add}) \\ \left(I_{he} + I_{ball} + I_z^{add}\right)\frac{d\omega}{dt} + \left(m_{he} + m_{ball} + m_y^{add}\right)\left(R_{Gy}\frac{du}{dt} + R_{Gx}\omega u\right) = M_G + M_B + M_T + M_A \\ m_i(d^2x_i/dt^2) = T_{xi+1} - T_{xi} + G_{xi} + \left(F_D^i + F_D^{i+1}\right)/2 \quad i = 1,\ldots,n \\ m_i(d^2y_i/dt^2) = T_{yi+1} - T_{yi} + G_{yi} + \left(F_L^i + F_L^{i+1}\right)/2 \quad i = 1,\ldots,n \end{cases} \tag{30}$$

The above equation is a system of nonlinear ordinary differential equations, which can be solved by introducing boundary conditions. In this paper, the fourth-order Runge–Kutta method is used for the numerical solution. The reduced order treatment of Equation (30) is as follows:

$$\begin{cases} u_i = dx_i/dt \\ v_i = dy_i/dt \end{cases} \tag{31}$$

where $i = 1,\ldots,n$.

Let $Y = \begin{bmatrix} x_b & u & y_b & v & \theta & \omega & x_i & u_i & y_i & v_i \end{bmatrix}^T$, $\frac{dY}{dt} = f(t, Y)$, and the initial condition $Y(t_0) = Y_0$; the time step is Δt, the following is the iterative formula, and the numerical solution of Y over time can be found by continuously looping the calculation.

$$\begin{cases} k_1 = f\left(t_j, Y_j\right) \\ k_2 = f\left(t_j + \frac{\Delta t}{2}, Y_j + \frac{\Delta t}{2}k_1\right) \\ k_3 = f\left(t_j + \frac{\Delta t}{2}, Y_j + \frac{\Delta t}{2}k_2\right) \\ k_4 = f\left(t_j + \Delta t, Y_j + \Delta t \cdot k_3\right) \\ Y_{j+1} = Y_j + \frac{\Delta t}{6}(k_1 + 2k_2 + 2k_3 + k_4) \\ t_{j+1} = t_j + \Delta t \end{cases} \tag{32}$$

where $j = 0, 1, 2, 3, \ldots$, j increases until the end of the simulation.

3. Results and Discussion

3.1. System Swing Analysis

To verify the accuracy of the longitudinal dynamics model of the tethered balloon system described above, oscillation tests in the longitudinal plane of the scaled-down tethered balloon system were conducted. The test environment is closed and indoors to ensure that the system is not interfered with by air circulation; the test principle is shown in Figure 6. The tethered balloon is connected to the mooring car with the main cable, and another cable with a smaller line density is connected to the other end of the cable,

which can be opened quickly to unlock the other end of the cable, which is connected to the ground-fixed capstan, and through the control of the capstan, the main cable in the vertical direction is set to a certain angle. Then, when the system is stabilized, the unlocking buckle is opened so that the system swings in the longitudinal plane. For the motion of the tethered balloon system, the tension of the main cable and the pitch angle of the balloon are two important parameters; therefore, an attitude sensor is installed on the simulation pod to record the balloon attitude angle, and a tension sensor is installed at the bottom of the main cable to record the tension at the bottom of the cable. The basic parameters of the test system are shown in Table 3, in which the coordinate system used for the center of mass of the balloon, the center of buoyancy of the balloon, and the position of the main tether point is the body coordinate system.
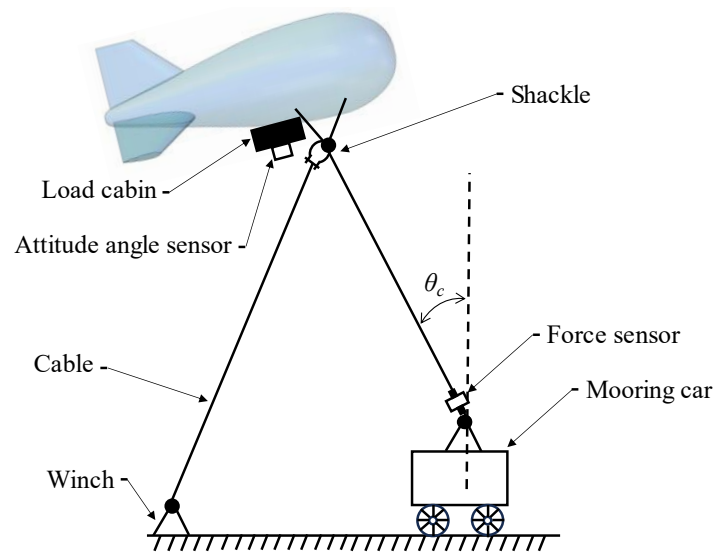

Figure 6. Principle of oscillation experiment.

Table 3. Basic parameters of scaled tethered balloon system.

| Parameters	Values	Parameters	Values
V_b	9.4 m^3	R_{Tx}	−1.085 m
L	5.6 m	R_{Ty}	1.12 m
m_{ball}	5.614 kg	ρ_A	1.204 kg/m^3
R_{Gx}	−0.613 m	ρ_b	0.229 kg/m^3
R_{Gy}	−0.367 m	ρ_c	5.9 g/m
R_{Bx}	0 m	d	3 mm
R_{By}	0 m	E	100 Gpa

Three sets of oscillation experiments were carried out for this scaled-down tethered balloon system, with the following conditions: cable length of 5 m, cable release angle of 30°; cable length of 10 m, cable release angle of 30°; cable length of 10 m, cable release angle of 20°. For the aggregate mass method, the more mass points that are selected, the closer the simulation results are to the real value, but the computational volume will also increase. In this paper, a series of mathematical models of cables with different numbers of mass points that can satisfy the calculation ability are established for the simulation analysis.

The experimental and simulation results are shown in Figure 7. With the growth of the cable, the change period of the pitch angle and the cable tension also become longer, and the amplitude decay becomes faster. The main reason for this is that the pitch angle of the balloon is obtained by the superposition of the rotation angle of the balloon relative to the main node and the rotation angle of the cable relative to the tethering point; a longer cable will make the rotation period of the cable around the tethering point longer, thus increasing

the change period of the pitch angle; and the change period of the tension at the bottom of the cable is positively correlated with the change period of the balloon's pitch angle. The period of change in the tension at the bottom of the cable is positively related to the period of change in the pitch angle of the balloon. As the initial inclination angle of the cable decreases, the pitch angle of the balloon and the period of the tension at the bottom of the cable remain unchanged, and the amplitude decreases because the initial inclination angle of the cable decreases, which results in a smaller amplitude of the cable oscillation. In the experiments and simulations, the change period of the pitch angle of the balloon and the tension at the bottom of the cable are close to each other, and the amplitude of the change in the simulation slightly increases compared with the experimental value, because the environment of the simulation is more ideal, and the balloon is not completely moving in the longitudinal plane in the experimental process, which results in the aerodynamic force of the balloon slightly increasing compared with that in the simulation, which leads to the small amplitude of the pitch angle of the balloon. The simulation results of the main tether model with different numbers of mass points are very close to the experimental results in terms of both the pitch angle of the balloon and the cable tension. In this paper, for the reduced-scale tethered balloon system with a main cable with a relatively short length, the number of cable mass points is five and meets the requirement for computational accuracy.

Figures 8 and 9 show the comparison of the results of the simulation and experiment with the cable length of 5 m and a cable release inclination angle of 30°. The number of cable mass points selected for the simulation is eight because the experiments cannot instantaneously release the cable, so that the beginning of the phase and the simulation results of the gap are large in the later stages of the swing system. The movement will gradually converge so that the characteristics of the various stages within a cycle will not be clear; so, the third cycle from the release of the cable is chosen for the analysis. The pitch angle of the balloon coincides with the tension at the bottom of the cable and the swing of the cable, and $t_1 \sim t_8$ are different points in the cycle.

The cable swings to the furthest point of the balloon at t_1 and the pitch angle velocity is at its maximum value; the pitch angle continues to increase and the cable tension continues to decrease until t_2, when the angular velocity decreases to zero and the balloon pitch angle reaches the maximum value. At t_3, the cable tension is reduced to the minimum value of the first half cycle. At t_4, the cable tension reaches the maximum value at this time; the pitch angle speed is zero; and the pitch angle of the balloon reaches the minimum value. At t_5, the cable is swinging towards the head of the balloon to the furthest point, and after that, it starts to swing towards the tail of the balloon. At t_6, the cable tension decreases to the minimum value in the whole cycle. At t_7, the cable tension increases to the maximum value in the second half of the cycle, and at t_8, the cable swings to the furthest point in the direction of the tail of the ball. In summary, the maximum and minimum values of the pitch angle of the balloon occur when the cable is swinging in the direction of the ball head. The maximum value of the cable tension occurs when the cable is about to swing to the furthest point in the balloon head direction when the pitch angle velocity is close to zero. As shown in Figure 9, the kinematic parameters of the experimental and simulated systems are very similar at all moments of the cycle.
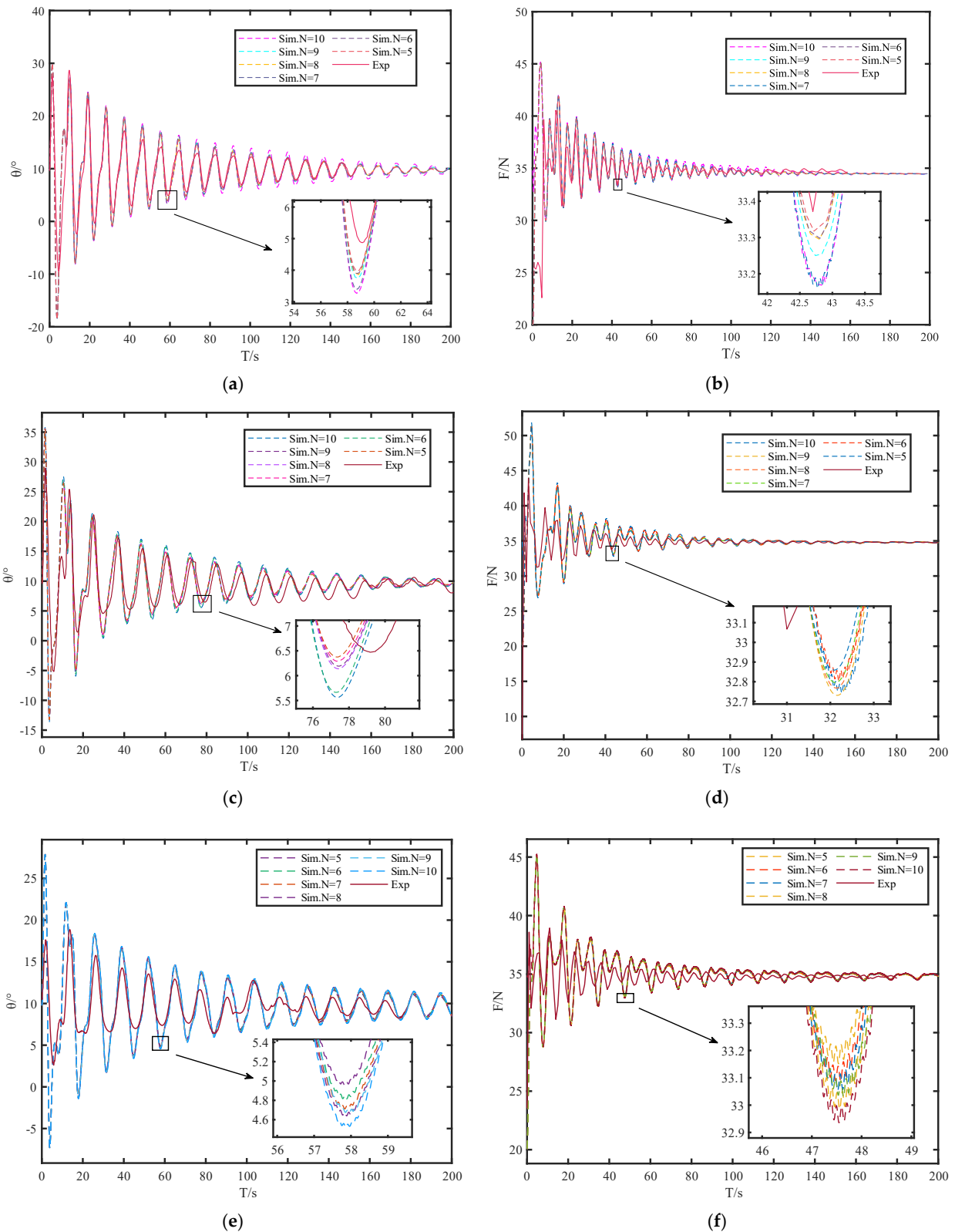
Figure 7. Comparison between simulation and experimental results of tethered balloon system oscillations. (**a**) Pitch with 5 m cable and 30° cable release inclination; (**b**) tension at the bottom of the cable with 5 m cable and 30° cable release inclination; (**c**) pitch with 10 m cable and 30° cable release inclination; (**d**) tension at the bottom of the cable with 10 m cable and 30° cable release inclination; (**e**) pitch with 10 m cable and 20° cable release inclination; (**f**) tension at the bottom of the cable with 10 m cable and 20° cable release inclination.
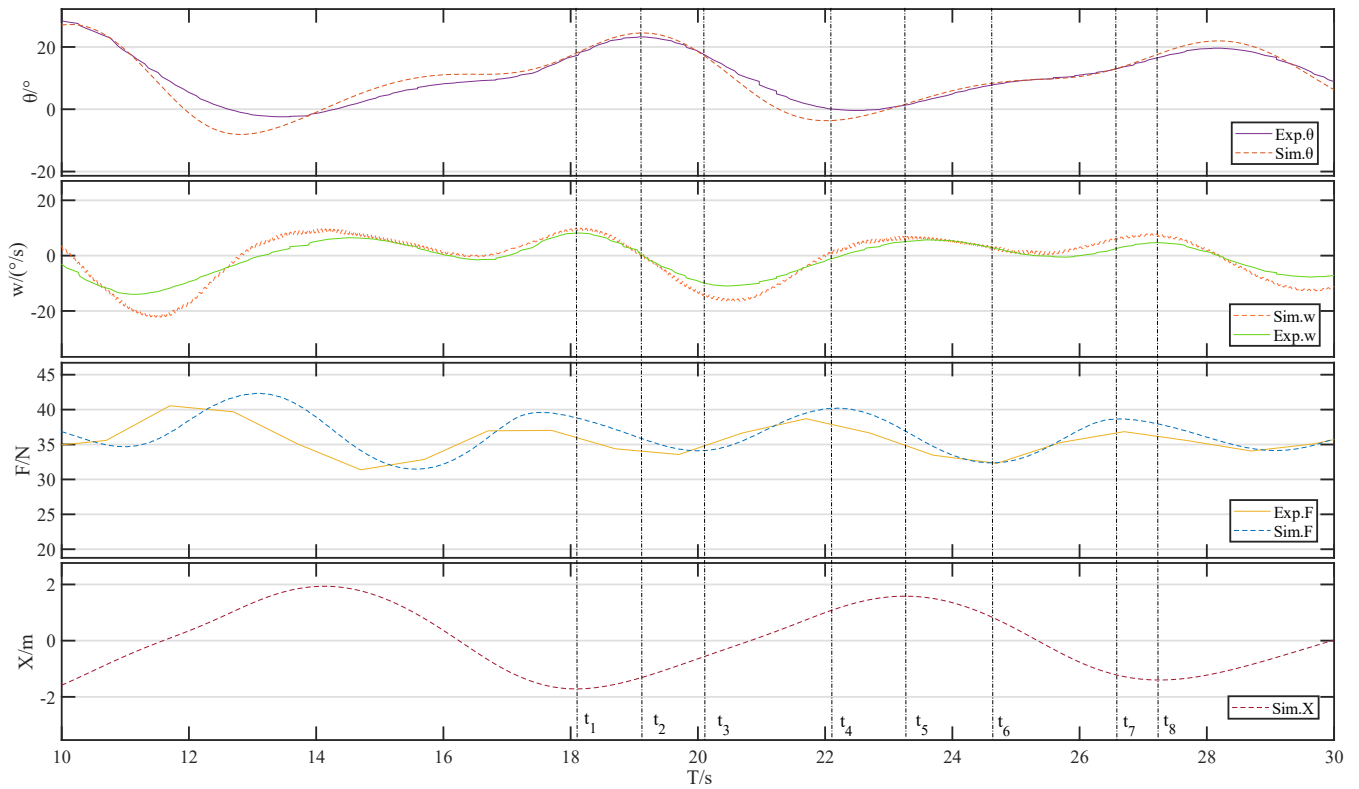
Figure 8. Comparison of simulation and experimental results for a cable length of 5 m and a cable release inclination of 30°.
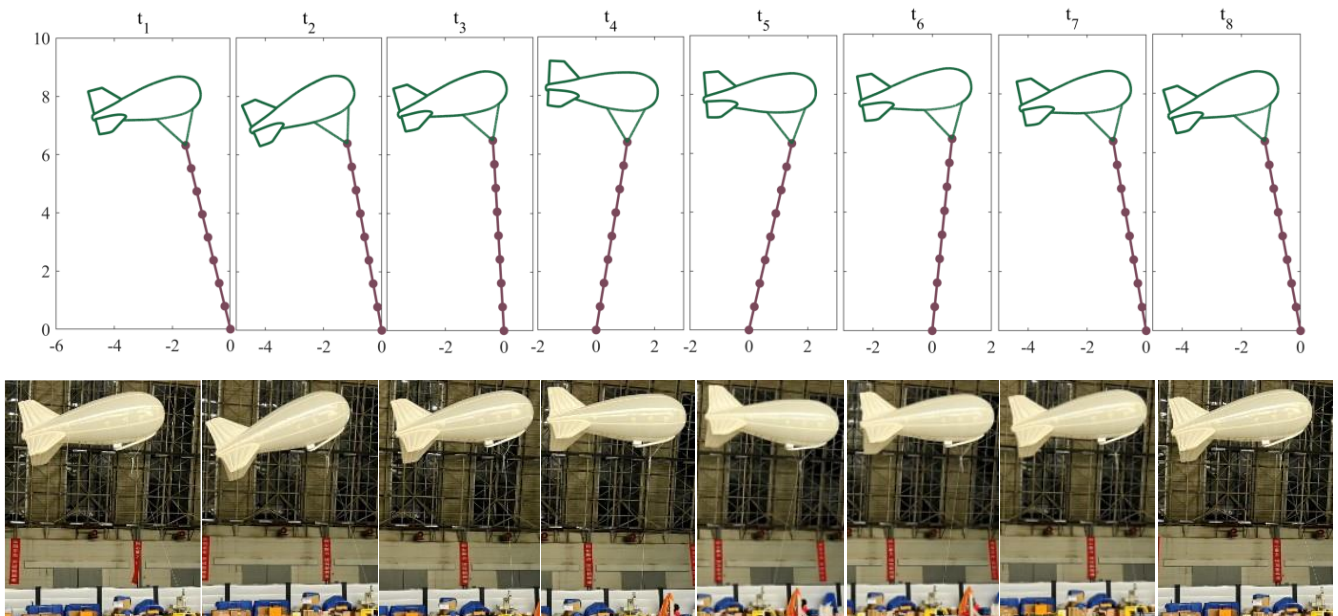
Figure 9. Tethered balloon swing comparison.

3.2. Analysis of System Wind Field Response

Tethered balloon systems will encounter very complex wind fields in the airborne process, and the system response will be very different. The following is a study of different wind field responses of tethered balloons with the basic parameters shown in Table 4. The mooring is set on the ground at zero altitude, the tethered balloon is stationed at a height of 1 km without wind, and the air density at the altitude where the balloon is situated is 1.112 kg/m^3.

Table 4. Basic parameters of a tethered balloon system.

Parameters	Values	Parameters	Values
V_b	2439 m^3	R_{Tx}	1.956 m
L	36 m	R_{Ty}	12.22 m
m_{ball}	643.4 kg	ρ_A	1.112 kg/m^3
R_{Gx}	−2.754 m	ρ_b	0.229 kg/m^3
R_{Gy}	−3.08 m	ρ_c	95 g/m
R_{Bx}	0.4 m	d	10.5 mm
R_{By}	0.973 m	E	100 Gpa

3.2.1. Wind Speed Amplitude Analysis

The wind field environment with different amplitudes is often encountered by the tethered balloon system and is greatly affected by it. Inputting the horizontal step wind field with different amplitudes to the above-tethered balloon system, the wind speed starts to increase uniformly from the 10th second of the simulation and reaches the maximum value after 10 s. The results of the system response are shown in Figure 10; from top to bottom, the main tether point tension is F, the balloon pitch angle is θ, the pitch angle velocity is ω, the main tether point horizontal coordinate is X, the main tether point longitudinal coordinate is Y, and the horizontal wind velocity is V_x. Higher horizontal wind speeds will cause the aerodynamic forces on the balloon and cable to increase, and the cable is the only constraint on the system, so the cable tension will also increase. The force transmitted from the cable to the balloon through the main tether point is an important part of the balancing system, and will also increase as the aerodynamic force increases. The offset between the pitch angle of the balloon after stabilization in the wind field and the stable pitch angle in the windless state increases with the increase in the wind speed amplitude, and the larger the wind speed, the shorter the pitch angle vibration period and the slower the attenuation. The larger the wind speed amplitude, the larger the displacement of the balloon from the windless equilibrium position. In summary, if there are certain requirements for the stability of the pitch angle and the spatial position of the tethered balloon in the process of airborne operation, it is necessary to consider that the amplitude of the wind speed of the working environment of the system is small enough.

3.2.2. Analysis of the Rate of Change in Wind Speed

The speed of wind speed change also affects the tethered balloon system; the tethered balloon system is inputted with a horizontal step wind field, the wind speed increases from zero to the maximum value of the wind speed to increase the time, and the parameters of the system are recorded during the simulation. Figure 11 shows the simulation results; it can be seen that the speed of wind speed change on the final convergence value of the system parameters does not have a significant impact. The slower the wind speed changes, the later the balloon will reach the equilibrium position, and the balloon pitch angle velocity and pitch angle changes in the magnitude and frequency will be smaller, the cable tension changes in the magnitude will be smaller, and the system will be able to reach a stable state faster. To sum up, if the tethered balloon system is required to be more stable, it is necessary to consider that the tethered balloon is stationed in an environment where the wind speed changes slowly.
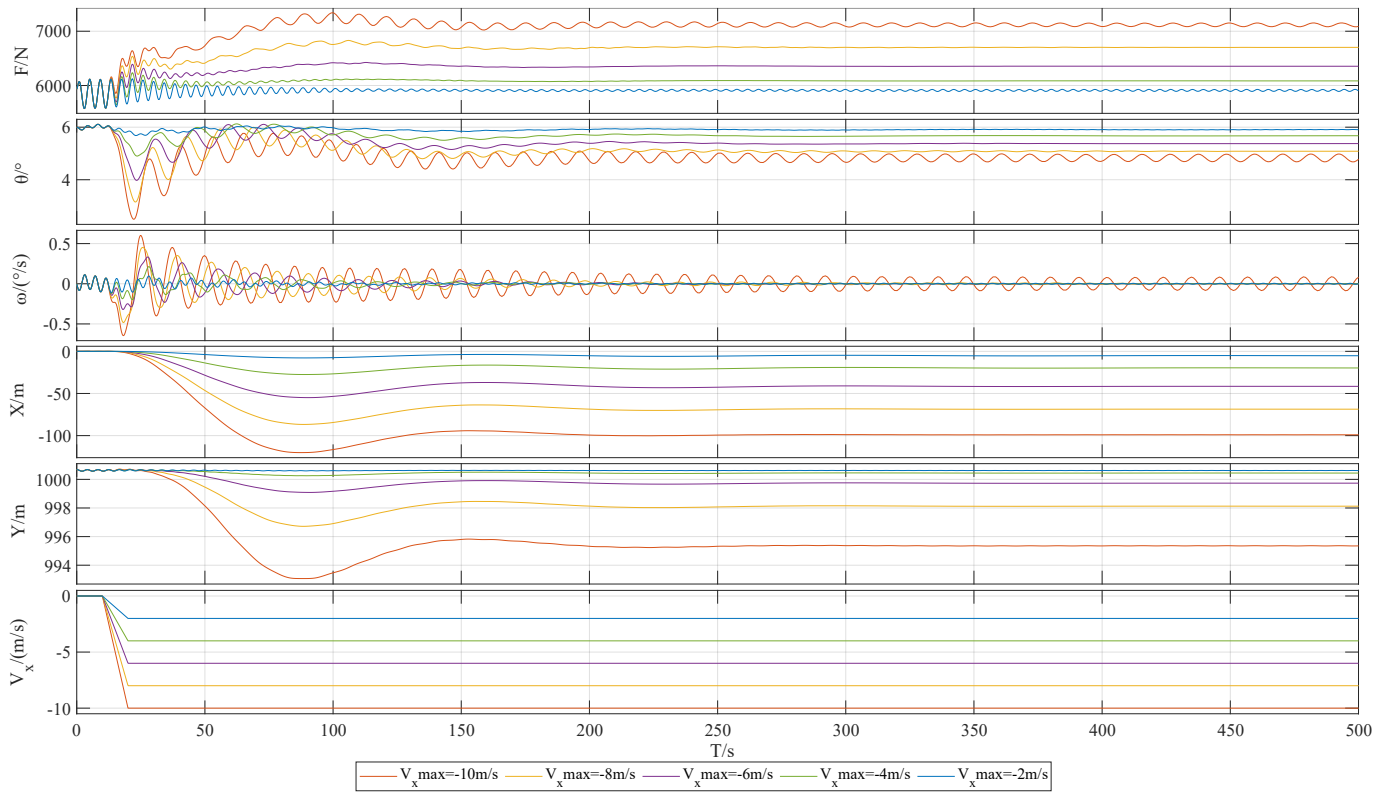
Figure 10. Response of the system with different wind speed amplitudes.
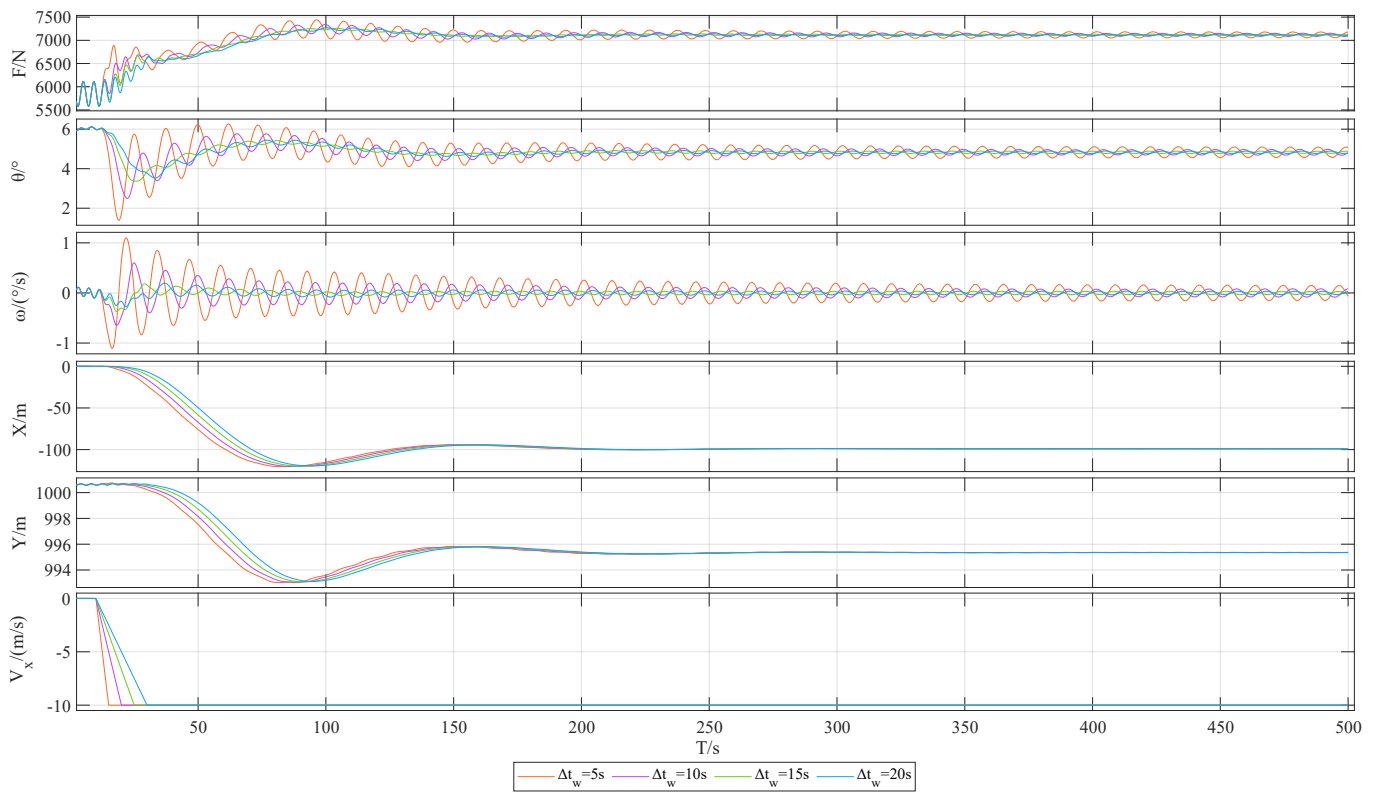

Figure 11. Response of the system with different rates of wind speed change.

3.2.3. Ascending Airflow Analysis

Tethered balloon systems are subjected to updrafts or downdrafts in the course of airborne operation, and their effect on a tethered balloon system during airborne operation

can be significant. Vertical airflow of different maximum magnitudes is applied to the balloon system with the basic parameters shown in Table 4. Figure 12 shows the motion response of the tethered balloon system when it encounters an updraft. The larger windward area of the balloon leads to a sharp increase in the aerodynamic force on the balloon, and since the aerodynamic force of the ball head portion is smaller than that of the balloon tail concerning the main tethering point, the balloon will show a more obvious bowing phenomenon, which is more and more obvious with the increase in the amplitude of the wind speed. In step-up airflow, the cable tension first increases sharply then decreases to a nearly stable state, and then gradually converges; the reason for this phenomenon is that the initial state of the balloon is a head-up state in the process of changing to a low state. There is a maximum aerodynamic force state that the wind field and the head and tail of the balloon near the perpendicular line of the state reach; the balloon is under the aerodynamic force of the rise of the balloon needed to reach its maximum value. For the same wind amplitude, the maximum tension of the cable under the updraft increases by 100.48% compared to that under the horizontal wind field, and the stabilized cable tension also increases by 56.1% compared to that of the horizontal wind field. Figure 13 shows the steady state of the tethered balloon system under different amplitudes of updrafts, and the balloon is enlarged in the figure for the convenience of illustrating the state of the balloon. Since the balloon is constrained by the cable and the constraint force is slanting to the lower part of the tail, the cable will be tilted in the direction of the ball head, and the tilting angle of the cable will be larger with the increase in the amplitude of the wind speed.
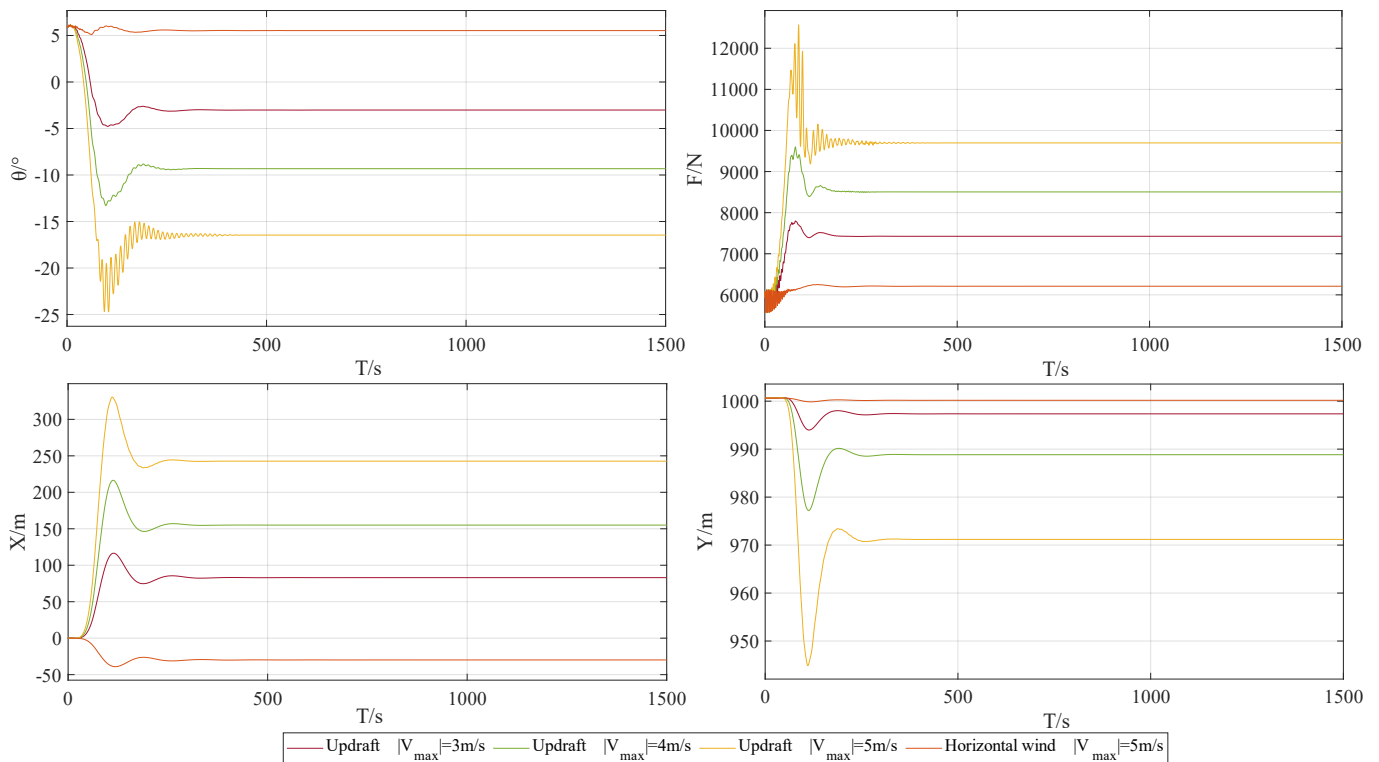

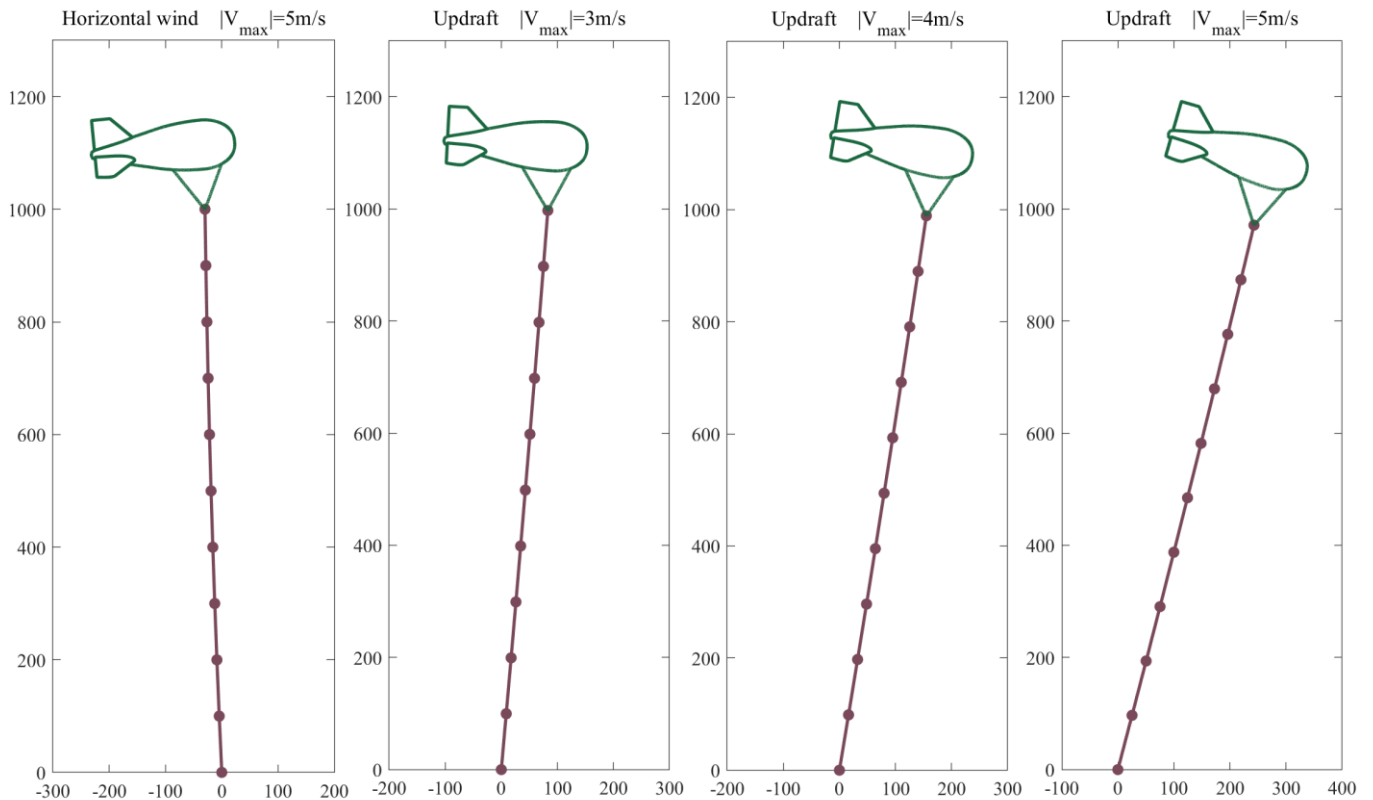**Figure 12.** System parameter response under rising airflow.

Figure 13. System steady-state position.

3.2.4. Descending Airflow Analysis

The response of the tethered balloon to different amplitudes of the step-down airflow is shown in Figure 14. The pitch angle of the balloon changes more when the wind speed amplitude is larger, because the aerodynamic force of the head part of the balloon is smaller than that of the tail part of the balloon concerning the main tethering point, but at this time, the aerodynamic force is pointing in the direction of the ground, so the balloon will exhibit a significant head-up phenomenon. Since the aerodynamic force on the balloon in the downdraft is pointing to the ground, the tension on the cable after the stabilization of the system is only 63.3% of the tension on the cable in a horizontal wind field with the same wind speed. The tethered balloon in the downdraft cable tension is also in the direction of the ball tail, so the cable is also tilted to the direction of the ball head. With the increase in wind speed, a 5 m/s downdraft can make the balloon horizontally offset by 600 m and the height of the balloon is only the same as the wind speed at the same level of the airflow at 75.3%; at this time, the risk of the balloon and the cable touching the ground is greatly increased. From Figure 14, it can be seen that after the amplitude of the falling air velocity reaches 5 m/s, the phenomenon where $\beta < \beta_1$ occurs, and the position of the rotational connection point between the balloon and the main bollard is transformed. Figure 15 shows the longitudinal section of the system after stabilization at different wind speed amplitudes in the downdraft wind field. To reduce the risk of cable breakage leading to the escape of the balloon as well as the risk of the balloon and cable hitting the ground, the balloon is avoided as much as possible in the vertical airflow.
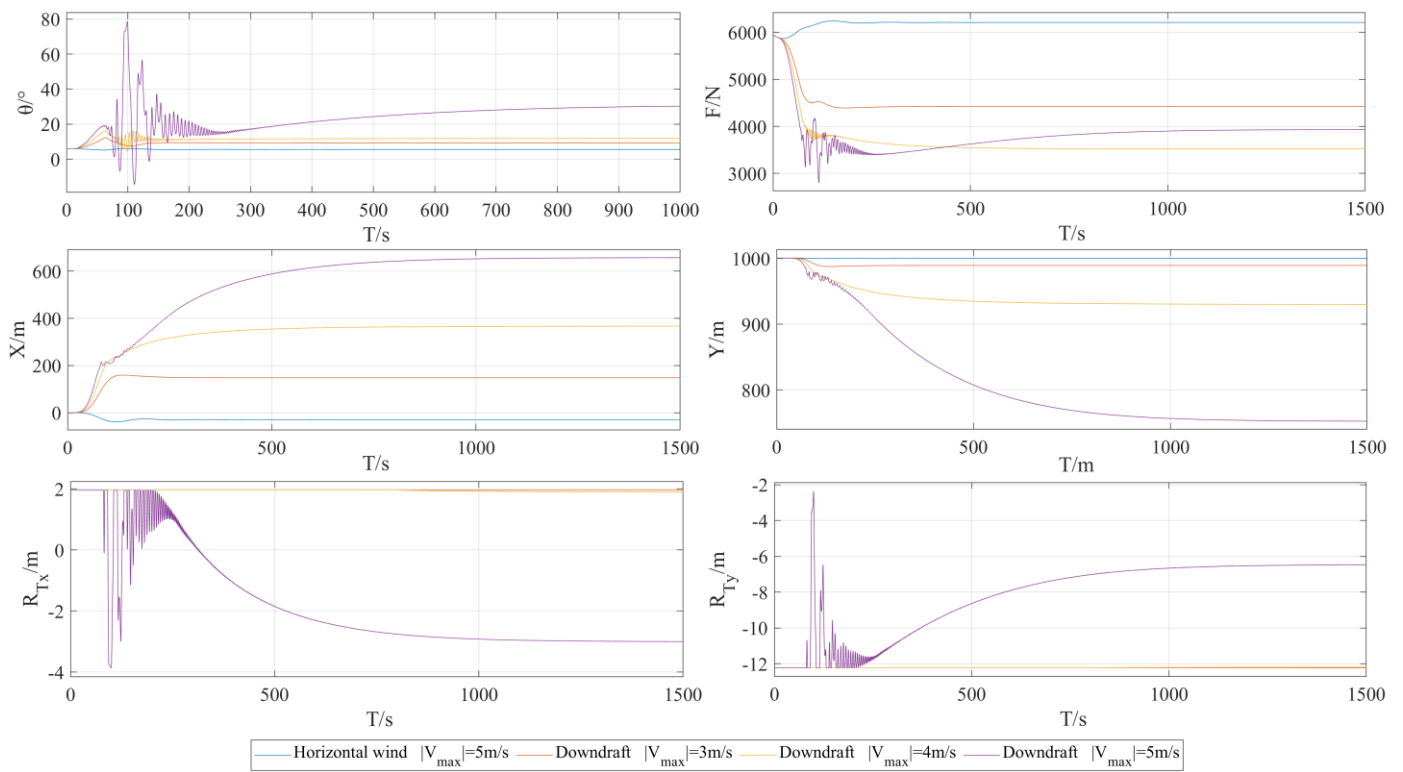
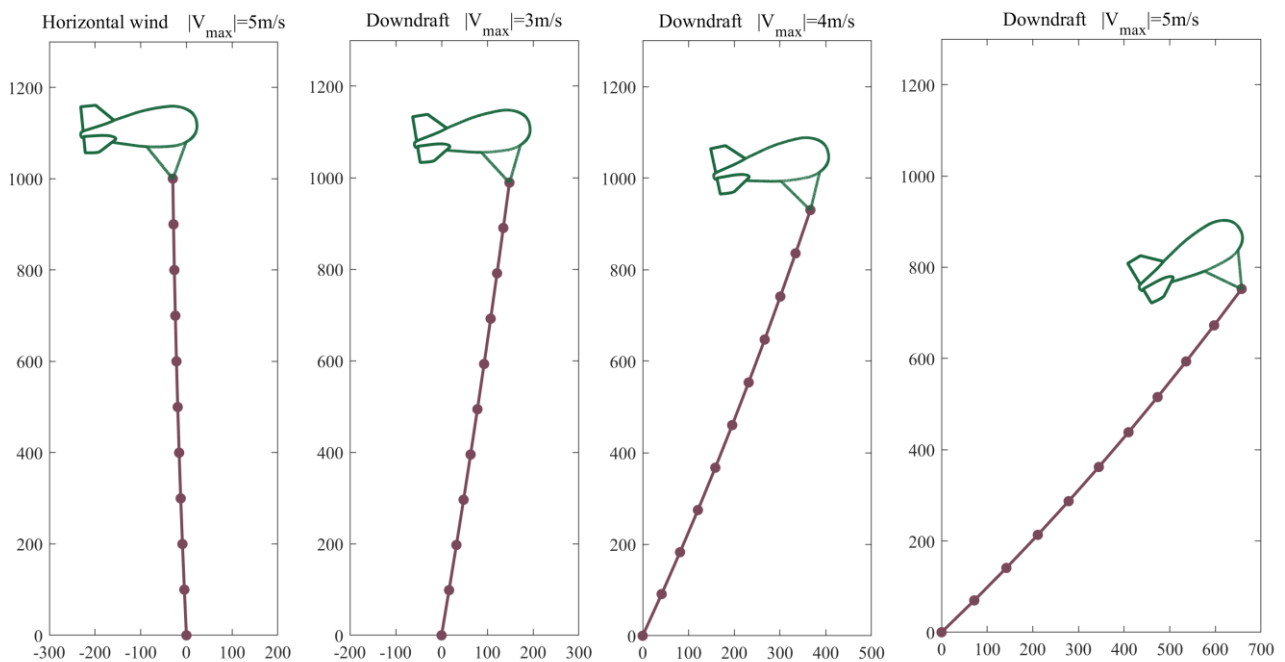**Figure 14.** System parameter response under falling airflow.

Figure 15. System steady-state position.

4. Conclusions

This paper investigates the effect of the wind field environment on the tethered balloon system and finds a suitable wind field environment for the tethered balloon system when in airborne flight. Firstly, the aerodynamic forces on the balloon during stationary flight were calculated in detail, and the differential equations for the dynamics of the tethered balloon system were established by applying the lumped mass method to simplify the cable model. Then, the swinging experiment of the tethered balloon system was carried out

to verify the accuracy of the simulation model. Finally, based on the above dynamic model, the response of the tethered balloon system in terms of different parameters under various wind fields was analyzed, which provides theoretical guidance for the safe stationary flight of the tethered balloon system.

1. In a horizontal step wind field, the larger the maximum wind speed, the higher the cable tension, the higher the cable inclination, the faster the wind speed changes, and the longer the time required for the system to stabilize.
2. When the tethered balloon system is in an updraft, the balloon shows a low head phenomenon and the tether is tilted towards the head direction, and the tension of the cable will increase dramatically, with the maximum value increasing by 100.48% compared with that in a horizontal wind field, which greatly increases the risk of the balloon escaping.
3. When the tethered balloon system is in descending airflow, the balloon shows the phenomenon of lifting, and the cable is also tilted to the direction of the balloon head. The tension of the cable is reduced to 63.3% of the horizontal wind field, but the height of the balloon is only 75.3% of the horizontal wind field, so the system's chances of touching the ground are increased.

Author Contributions: Conceptualization, C.P. and Z.H.; methodology, C.P.; software, C.P.; validation, C.P., K.S. and S.C.; formal analysis, C.P.; investigation, Z.H.; resources, Z.H.; data curation, C.P.; writing—original draft preparation, C.P.; writing—review and editing, K.S.; visualization, C.P.; supervision, Z.H.; project administration, Z.H.; funding acquisition, Z.H. All authors have read and agreed to the published version of the manuscript.

References

1. Ferrero, L.; Ritter, C.; Cappelletti, D.; Moroni, B.; Močnik, G.; Mazzola, M.; Lupi, A.; Becagli, S.; Traversi, R.; Cataldi, M.; et al. Aerosol Optical Properties in the Arctic: The Role of Aerosol Chemistry and Dust Composition in a Closure Experiment between Lidar and Tethered Balloon Vertical Profiles. *Sci. Total Environ.* **2019**, *686*, 452–467. [CrossRef]
2. Guan, X.; Zhang, N.; Tian, P.; Tang, C.; Zhang, Z.; Wang, L.; Zhang, Y.; Zhang, M.; Guo, Y.; Du, T.; et al. Wintertime Vertical Distribution of Black Carbon and Single Scattering Albedo in a Semi-Arid Region Derived from Tethered Balloon Observations. *Sci. Total Environ.* **2022**, *807*, 150790. [CrossRef] [PubMed]
3. Sikand, M.; Koskulics, J.; Stamnes, K.; Hamre, B.; Stamnes, J.J.; Lawson, R.P. Mixed Phase Boundary Layer Clouds Observed from a Tethered Balloon Platform in the Arctic. *Proc. AIP Conf. Proc.* **2013**, *1531*, 540–543.
4. Kai, K.; Kawai, K.; Ohara, K.; Minamoto, Y.; Jin, Y.; Maki, T.; Noda, J.; Shiina, T.; Davaanyam, E. Mass-Extinction Conversion Factor (MECF) over the Gobi Desert by a Tethered-Balloon-Based OPC and a Ceilometer. *SOLA* **2023**, *19*, 269–273. [CrossRef]
5. Alsamhi, S.H.; Gupta, S.K.; Rajput, N.S. Performance Evaluation of Broadband Service Delivery via Tethered Balloon Technology. In Proceedings of the 2016 11th International Conference on Industrial and Information Systems (ICIIS), Roorkee, India, 3–4 December 2016; pp. 133–138.
6. Wei, Z.; Bao, Z.; Zhang, Y. The Application and Development of Tethered Cables. *Opt. Fiber Electr. Cable Their Appl.* **2013**, *6*, 1–3.
7. Qi, J.; Xiaodong, L.; Fantao, M.; Na, L. The Design and Performance Analysis of VLF Tethered Balloon Cable Antenna. *Chin. J. Radio Sci.* **2021**, *36*, 775–780.
8. Wang, Y.; Jia, Y.; Chen, Z.; Han, Y.; Yang, C. Static and Dynamic Simulation of Tethered Airship. *Spacecr. Recovery Remote Sens.* **2012**, *33*, 93–99.
9. Hong-quan, L.; Lei, W. Dynamic Simulation Analysis of Wind-Resistant Performance for a Tethered Balloon. *J. Astronaut. Metrol. Meas.* **2014**, *34*, 29.

10. Costello, H.M.; Kuo, K.A.; Hunt, H.E.M. Stability Analysis of an Aerodynamically Shaped High-Altitude-Balloon Tether. In Proceedings of the International Conference on Noise and Vibration Engineering, Leuven, Belgium, 17–19 September 2012; pp. 3003–3012.
11. Jang, Y.; Zhang, T.; Qu, Z. Influence of Tail Configuration on Aerodynamic Characteristics of Small Tethered Balloon. *Comput. Simul.* **2022**, *39*, 28–34.
12. Badesha, S.; Bunn, J. Dynamic Simulation of High Altitude Tethered Balloon System Subject to Thunderstorm Windfield. In Proceedings of the AIAA Atmospheric Flight Mechanics Conference and Exhibit, Monterey, CA, USA, 5 August 2002; American Institute of Aeronautics and Astronautics: Reston, VA, USA, 2002.
13. Mukherjee, D.; Sharma, I.; Gupta, S.S. Dynamics and Stability of Variable-Length, Vertically-Traveling, Heavy Cables: Application to Tethered Aerostats. *J. Aircr.* **2019**, *56*, 68–84. [CrossRef]
14. Zhang, D.; Zhang, T.; Cui, Y.; Chen, C.; Wang, S. Sensitivity Analysis of Aerodynamic Parameters of Stratospheric Tethered Balloon. *Acta Aeronaut. Astronaut. Sin.* **2022**, *43*, 176–185.
15. Aglietti, G.S. Dynamic Response of a High Altitude Tethered Balloon System. *J. Aircr.* **2009**, *46*, 2032–2040. [CrossRef]
16. Pastor-Rodríguez, A.; Sánchez-Arriaga, G.; Sanjurjo-Rivo, M. Modeling and Stability Analysis of Tethered Kites at High Altitudes. *J. Guid. Control Dyn.* **2017**, *40*, 1892–1901. [CrossRef]
17. Zhang, H.; Yang, Y.; Cai, R. Dynamics Simulation of a Folding Wing Unmanned Aerial Vehicle with the Parachute System Assisted Launching. *Proc. Inst. Mech. Eng. Part G J. Aerosp. Eng.* **2023**, *237*, 1351–1368. [CrossRef]
18. Zhang, H.; Yang, Y.; Cai, R.; Zhao, R. Numerical Simulation of the Dynamic Launching Process for High-Altitude Balloons. *Adv. Space Res.* **2021**, *68*, 3677–3699. [CrossRef]
19. Tuckerman, L. *Inertia Factors of Ellipsoids for Use in Airship Design*; US Government Printing Office: Washington, DC, USA, 1925.
20. Williams, P.; Sgarioto, D.; Trivailo, P. Optimal Control of an Aircraft-Towed Flexible Cable System. *J. Guid. Control Dyn.* **2006**, *29*, 401–410. [CrossRef]